The Journal of Immunology

Dimeric FcγR Ectodomains as Probes of the Fc Receptor Function of Anti-Influenza Virus IgG

Bruce D. Wines, Hillary A. Vanderven, Sandra E. Esparon, Anne B. Kristensen, Stephen J. Kent and P. Mark Hogarth

J Immunol 2016; 197:1507-1516; Prepublished online 6 July 2016;
doi: 10.4049/jimmunol.1502551
http://www.jimmunol.org/content/197/4/1507

The Journal of Immunology is published twice each month by
The American Association of Immunologists, Inc.,
9650 Rockville Pike, Bethesda, MD 20814-3994.

Print ISSN: 0022-1767 Online ISSN: 1550-6606.

Dimeric FcγR Ectodomains as Probes of the Fc Receptor Function of Anti-Influenza Virus IgG

Bruce D. Wines,*,†,‡ Hillary A. Vanderven,§ Sandra E. Esparon,* Anne B. Kristensen,§ Stephen J. Kent,§,¶,‖ and P. Mark Hogarth*,†,‡

Ab-dependent cellular cytotoxicity, phagocytosis, and Ag presentation are key mechanisms of action of Abs arising in vaccine or naturally acquired immunity, as well of therapeutic mAbs. Cells expressing the low-affinity FcγRs (FcγRII or CD32 and FcγRIII or CD16) are activated for these functions when receptors are aggregated following the binding of IgG-opsonized targets. Despite the diversity of the Fc receptor proteins, IgG ligands, and potential responding cell types, the induction of all FcγR-mediated responses by opsonized targets requires the presentation of multiple Fc regions in close proximity to each other. We demonstrated that such "near-neighbor" Fc regions can be detected using defined recombinant soluble (rs) dimeric low-affinity ectodomains (rsFcγR) that have an absolute binding requirement for the simultaneous engagement of two IgG Fc regions. Like cell surface–expressed FcγRs, the binding of dimeric rsFcγR ectodomains to Ab immune complexes was affected by Ab subclass, presentation, opsonization density, Fc fucosylation, or mutation. The activation of an NK cell line and primary NK cells by human IgG-opsonized influenza A hemagglutinin correlated with dimeric rsFcγRIIIa binding activity but not with Ab titer. Furthermore, the dimeric rsFcγR binding assay sensitively detected greater Fc receptor activity to pandemic H1N1 hemagglutinin after the swine influenza pandemic of 2009 in pooled human polyclonal IgG. Thus these dimeric rsFcγR ectodomains are validated, defined probes that should prove valuable in measuring the immune-activating capacity of IgG Abs elicited by infection or vaccination or experimentally derived IgG and its variants. ***The Journal of Immunology*****, 2016, 197: 1507–1516.**

The Fc-mediated effector functions of Abs are being increasingly appreciated as making key contributions to Ab efficacy against infectious agents. Fc-mediated function is essential for the full protective activity of Abs to many viruses (1–7), including HIV (8–10), simian HIV (11), HSV type 2 (4), and influenza (6). Moreover, a broadly neutralizing Ab (6F12) directed against the influenza A hemagglutinin (HA) stalk region required FcγR engagement for full protective activity (12), making the stalk region a promising vaccine target for neutralization (13) and Fc receptor (FcR)-mediated protection (14, 15). Thus, although HA inhibition by neutralizing Ab is the standard measure of a protective response to vaccination against influenza (16), Ab-dependent cellular phagocytosis (17), Ab-dependent cellular cytotoxicity (7, 18, 19), and other FcγR-dependent functions also contribute to immunity and form part of the optimal vaccine response (14, 20). The capacity of IgG to facilitate FcγR-mediated Ag presentation (21) and induce dendritic cell activation (22) provides another mechanism for Fc-dependent effects in immunity to some infectious agents (23) and immunity more generally (24). Taken together, effector functions triggered by the engagement of FcRs are key contributors to the efficacy of Ab-mediated protection in natural immunity, vaccine responses, and treatments with therapeutic Abs (25, 26).

Despite being fundamental to Ab-mediated immunity, FcR-mediated effector functions are difficult to define and measure, in part because of the different receptors and the plethora of cell types and responses that may be generated. Despite this diversity, FcR activation of cells occurs when Abs aggregated by complexing with Ag present a cluster of Fc regions that cross-link FcRs and trigger subsequent downstream signaling.

Structural studies of the interaction of the human IgG1 Ab Fc region with its various cellular receptors [FcγRI (27, 28), FcγRIIa (29, 30), FcγRIIb (31), and FcγRIIIa (32, 33)], in combination with biosensor studies, defined the atomic basis of the 1:1 interactions of single FcR ectodomains with an IgG1-Fc (34, 35). However, the physiological interaction of IgG immune complexes (ICs) and FcγR requires avid binding of the complex through the display of multiple Fc regions of "near-neighbor" IgGs to engage and cluster multiple FcγRs on the cell surface (36). Hence, differences in the opsonization of targets by different IgGs influence interactions with FcγRs, chiefly by the density, size (37, 38), and topology of presentation of the Fc regions. Although not easily predicted, these effects may profoundly affect cellular functions (39). Thus, how Ag-bound Abs are presented for sensing by FcγRs underpins effector functions, such as Ab-dependent cellular cytotoxicity and Ab-dependent cellular phagocytosis, but is not simple to quantitate experimentally. Cell-based assays for such key cellular responses (40–45) are difficult to standardize, so there is a need for an assay that simply evaluates the capacity of an immune complex (IC) to present Fcs for avid binding by FcγRs.

In an attempt to recapitulate the avid sensing of ICs by cell surface FcγRs, our approach used a single, biotin-tagged polypeptide containing two FcγR ectodomains where the two Fc-binding modules

*Centre for Biomedical Research, Burnet Institute, Melbourne, Victoria 3004, Australia; †Department of Immunology, Monash University Central Clinical School, Melbourne, Victoria 3004, Australia; ‡Department of Pathology, The University of Melbourne, Melbourne, Victoria 3052, Australia; §Department of Microbiology and Immunology, Peter Doherty Institute for Infection and Immunity, The University of Melbourne, Parkville, Victoria 3052, Australia; ¶Australian Research Council Centre of Excellence in Convergent Bio-Nano Science and Technology, The University of Melbourne, Parkville, Victoria 3052, Australia; and ‖Melbourne Sexual Health Centre, Infectious Diseases Department, Alfred Health, Monash University Central Clinical School, Melbourne, Victoria 3004, Australia

Received for publication December 8, 2015. Accepted for publication June 3, 2016.

This work was funded by Australian National Health and Medical Research Council Award ACH2 and the Victorian Operational Infrastructure Scheme.

Address correspondence and reprint requests to Prof. P. Mark Hogarth, Centre for Biomedical Research, Burnet Institute, 85 Commercial Road, Melbourne, VIC 3004, Australia. E-mail address: mark.hogarth@burnet.edu.au

Abbreviations used in this article: A450nm, absorbance at 450 nm; C.I., confidence interval; FcR, Fc receptor; HA, hemagglutinin; HSA, human serum albumin; IC, immune complex; rs, recombinant soluble; TNP, trinitrophenyl; WT, wild-type.

www.jimmunol.org/cgi/doi/10.4049/jimmunol.1502551

were linked by the FcγRIIa membrane proximal stalk region. In this approach, the selective binding of these dimeric FcγR ectodomains to ICs is dependent on the presentation of pairs of "near-neighbor" Fc regions by the IC to bind both ectodomain modules of the receptor dimer. These dimeric recombinant soluble (rs)FcγR probes recapitulated many properties of the cell surface receptors, including selectivity for binding IgG subclasses and the binding affinities and specificities of the allelic forms of FcγRIIIa and FcγRIIa. Furthermore, the afucosyl form of IgG1 was more active in dimeric rsFcγRIIIa binding than the normally glycosylated mAb. The binding of the dimeric rsFcγRIIIa probe correlated with NK activation by ICs. This assay is useful for evaluating the functional activity of IgGs binding different Ags and epitopes and in different forms, including mutants, subclasses, and glycoforms.

Materials and Methods

Reagents

Abs and proteins. Albumin, bovine Fraction V, and human IgG1, IgG2, IgG3, and IgG4 myeloma proteins were from Sigma-Aldrich. Human IgG1 mAb b12, its LALA mutant, LL(234–235)AA, and afucosyl variant were a gift from Prof. Dennis Burton (The Scripps Institute, La Jolla, CA). High Sensitivity Streptavidin-HRP conjugate was from Pierce (Thermo Scientific, Melbourne, Australia). IgG capture reagent was AffiniPure $F(ab')_2$ goat anti-human IgG-$F(ab')_2$ specific (Jackson ImmunoResearch, West Grove, PA). Human serum albumin (HSA), IvIg: INTRAGAM P (i.v. Ig (normal IgG, 6%), and IvIg:Sandoglobulin (2004 to 2010) were from bioCSL (Parkville, Australia). Influenza A virus HA protein was from Sinobiological (Shanghai, China), polyclonal rabbit anti-human IgG-HRP (Dako, Sydney, Australia), and 3,3′,5,5′-tetramethylbenzidine ELISA substrate (Life Technologies/Thermofisher, Melbourne, Australia).

Generation of BirA ligase–expressing cell lines. A pIREShygro expression vector containing BirA ligase with a C-terminal endoplasmic reticulum–targeting sequence [a gift from Dr. Amanda Gavin, The Scripps Institute, La Jolla, CA, with the insert from pDisplay-BirA-ER, a gift from Alice Ting, Massachusetts Institute of Technology Cambridge, MA (Addgene plasmid #20856) (46)] was transfected using Lipofectamine 2000 into HEK293EBNA cells and Expi293F cells (Thermo Fisher Scientific, Scoresby, Australia). Transfectants were selected with 100 μg/ml hygromycin and maintained in 50 μg/ml hygromycin. Expression using Expi293F-BirA cells followed the manufacturer's instructions for Expi293F cells. All hexahistidine-tagged proteins were purified by affinity chromatography on a TALON Superflow (BD Biosciences), as described previously (47).

RsFcγRIIa H131 ectodomain monomer and dimer expression constructs. All PCR reactions were performed using polymerase Pwo (Roche) or AccuPrime Pfx polymerase (Thermo Fisher). All other DNA-modifying enzymes were from New England Biolabs. The construction of a vector encoding monomeric rsFcγRIIa with a hexahistidine and biotin ligase target tag used amplification from the cDNA encoding FcγRIIa (clone Hu3.0, which includes a unique BamHI site) (48) with the product ligated to a codon-optimized sequence encoding a hexahistidine tag and biotin ligase target sequence (GenScript USA) so that the C-terminal sequence was GPGSSSHHHHHHPGGGLNDIFEAQKIEWHE, with the underlined residue corresponding to Gly^{175} of FcγRIIa (i.e., Gly^{211} of the precursor, RefSeq NP_001129691). To make a dimerized receptor construct, the clone Hu3.0 was amplified (using the equivalent of primers GTA*GCTCCCCCAAAGGCTG* and GGG*TGAAGAGCTGCCCATG* (GGG corresponding to the antisense for the codon of FcγRIIa Pro^{179} [i.e., Pro^{215} of the precursor]); the blunt product was ligated together with T4 ligase, and a correctly orientated tandem dimer of the receptor ectodomain was subcloned. Using standard molecular biology, a BamHI fragment from this construct was subcloned into the unique BamHI site in the monomeric vector to produce a vector containing the endogenous FcγIIa leader, the dimeric ectodomain sequence described above, and the C-terminal GPGSSSHHHHHHPGGGLNDIFEAQKIEWHE tag. The monomeric or dimeric rsFcγRIIa proteins were expressed from pAPEX-3p-X-DEST (pBAR424) or pCR3-DEST, as described previously (49, 50), and using HEK293EBNA-BirA cells or Expi293F-BirA cells, respectively.

RsFcγRIIIa monomer and dimer expression constructs. Codon-optimized sequences encoding the ectodomains of rsFcγRIIIa Val^{158} and Phe^{158} with the N-terminal sequence MVLSLLYLLTALPGISTEDLPKAVVFL and the C-terminal sequence QGPSMGSSSPGPGSSSHHHHHHPGGGLNDIFEAQKIEWHE (underlined Q corresponds to residue Gln^{172}, or Gln^{191} of the precursor, RefSeq NP_000560) were synthesized by GeneArt (Invitrogen) and transposed by BP clonase reaction into pENTR1A (Invitrogen). The native protein leader sequences in these constructs were replaced with MVLSLLYLLTALPGIST and validated using Signal P (51). PCR with the primer pairs 5′-AGCGAGGACCTGCCTAAGGCCGT-3′ and 5′-CGGAGAACTAGAGCCCATGCTG-3′ and 5′-CGGAGAACTAGAGCCCATGCTG-3′ and 5′-GGGCCTGGCAGCTCCTCTC-3′ generated an ectodomain and ectodomain in vector product, respectively, which were ligated to generate the tagged dimeric rsFcγRIIIa ectodomain sequences. The underlined residues of QGPSMGSSSPSE are encoded by the linking sequence between the tandem ectodomains; Q corresponds to residue Gln^{172} of the first ectodomain, and E corresponds to residue Glu^{1} of the tandem ectodomain. After sequence validation, LR clonase reactions (Invitrogen) with pCR3-DEST generated expression vectors encoding monomeric and dimeric forms of rsFcγRIIIa Val^{158} and Phe^{158} proteins. These recombinant receptors were then expressed in Expi293F-BirA cells as described above.

RsFcγRIIa Arg^{131} monomer and dimer expression constructs. Similarly to the rsFcγRIIIa monomer and dimer expression constructs, a codon-optimized sequence encoding an N-terminal leader sequence MVLSLLYLLTALPGILSA and C-terminal sequence GSSSPGSSSHHHHHHPGGGLNDIFEAQKIEWHE, with the underlined residue corresponding to Gly^{175} of FcγRIIa, was used to flank the optimized codons for mature FcγRIIa Arg^{131} codons 1–175. Using PCR, the DNA encoding the ectodomain module (30) (PDB ID code: 3RY5) was joined to itself in tandem, such that the encoded junction of the duplicated ectodomain modules was ITVQVPSMGSSSPAAPPK (the linking peptide sequence between the modules is underlined); the first module retained the sequence for the leader, and the second module retained the sequence for the C-terminal tag. Expression of this pCR3-based construct used Expi293F-BirA cells, as described above.

Ab expression constructs. The production of a chimeric IgG1 comprising a mouse leader and VH sequence (from TIB142 anti-trinitrophenyl [TNP]; American Type Culture Collection) joined to a human IgG1 C region sequence was described previously (49). Chimeric anti-TNP κ L chain consisting of TIB142VL and human constant κ was produced from a codon-opsonized construct synthesized by Bioneer Pacific (Kew, Australia). An IgG4 chimeric H chain comprising TIB142 leader and VH and IgG4 constant (Bioneer Pacific) sequence was codon optimized, synthesized, and transferred into pCR3. Likewise, the TNP-specific mouse VH sequence was joined to a human IgG2 genomic C region sequence (accession no. J00230) using standard molecular biology techniques, and the chimeric Ab sequence was subcloned into pCR3.

FcγR-binding assays using dimeric rsFcγR-biotin. IgG capture reagent, $F(ab')_2$ goat anti-human IgG, $F(ab')_2$ (10 μg/ml), TNP-BSA (20 μg/ml), or influenza A HA (1 μg/ml) was prepared in PBS and adsorbed (50 μl/well) to plates (MaxiSorp; Nunc). For the analysis of patient samples or IvIg, wells (typically three) were directly coated with 5 μg/ml IvIg (INTRAGAM P), and signals from these wells were used to normalize the FcR activity of the test samples. Coated wells were subsequently blocked with PBS containing 1 mM EDTA and 1% (w/v) BSA (Fraction V; Sigma-Aldrich); 1% HSA was used if subsequent testing was of patient or IvIg samples. IgG samples (typically diluted from a starting concentration of 1–5 μg/ml) were incubated with the IgG capture reagent, TNP-BSA, or Ag-coated wells for 1 h at 37°C. Plates were washed five times with PBS containing 0.05% Tween-20. The Ab-bound plates were incubated with 0.2 μg/ml purified dimeric rsFcγRIIa-biotin or 0.1 μg/ml purified dimeric rsFcγRIIIa-biotin, in PBS diluent containing 1 mM EDTA, 0.05% Tween-20, and 1% (w/v) BSA for 1 h at 37°C. After five cycles of filling and emptying with wash buffer, High Sensitivity Streptavidin-HRP (Thermo Fisher), 1/10,000 in diluent buffer, was added for 1 h at 37°C, followed by 8–10 cycles of filling and emptying with wash buffer and development with TMB Single Solution (Thermo Fisher). The reaction was stopped by addition of an equal volume of 1 M HCl, and absorbance at 450 nm (A450nm) was determined immediately. Delayed determination of absorbance can produce an apparent prozone effect artifact because precipitation of the colorimetric product occurs at high concentration. Bound IgG was measured using polyclonal rabbit anti-human IgG-HRP (Agilent Technologies-Dako, 1/10,000 dilution; Sigma-Aldrich, 1/20,000), and plates were blocked using HSA depleted of IgG by protein G chromatography (GE Life Technologies) or 1% FCS in PBS.

NK cell–activation assay. NK cell activation was measured by HA:anti-HA IC-dependent induction of intracellular IFN-γ and cell surface CD107a, as previously described (6, 7, 18, 52–54). Briefly, 96-well ELISA plates (Nunc, Rochester, NY) were coated with 600 ng of purified HA protein overnight at 4°C in PBS. The wells were washed five times with PBS and incubated with heat-inactivated (56°C for 1 h) sera/plasma or IvIg for 2 h at

37°C. Plates were washed seven times with PBS, and 10^6 PBMCs were added to each well. Healthy donor PBMCs were obtained from buffy packs provided by the Australian Red Cross. PBMCs were isolated by Ficoll-Paque PLUS (GE Healthcare, Madison, WI), washed with RPMI 1640 supplemented with 10% FCS, penicillin, streptomycin, and L-glutamine (Life Technologies, Grand Island, NY), frozen in FCS containing 10% DMSO, and stored in liquid nitrogen. Thawed PBMCs were washed twice with RPMI 1640 supplemented with 10% FCS, penicillin, streptomycin, and L-glutamine before addition to each well. Anti-human CD107a allophycocyanin-H7 Ab (clone H4B4; BD Biosciences, San Jose, CA), 5 μg/ml brefeldin A (Sigma-Aldrich), and 5 μg/ml monensin (Golgi Stop; BD Biosciences) were added to the cells and incubated for 5 h at 37°C with 5% CO_2. PBMCs were then incubated with 1 mM EDTA to minimize cell adherence to the plates, anti-human CD3 PerCP (clone SP34-2), and anti-human CD56 allophycocyanin (clone B159; both from BD Biosciences) for 30 min at room temperature in the dark. Cells were fixed with 1% formaldehyde (Sigma-Aldrich) for 10 min and permeabilized with FACS Permeabilizing Solution 2 (BD Biosciences) for 10 min. PBMCs were then incubated at room temperature for 1 h with IFN-γ Alexa Fluor 700 (clone B27; BD Biosciences) in the dark. Finally, cells were fixed with 1% formaldehyde and acquired on an LSR II flow cytometer (BD Biosciences).

The NK cell line NK-92 (55) expressing human FcγRIIIa Val^{158} (GFP-CD16 [176V] NK-92) was used to perform some of the NK cell–activation assays and was kindly provided by Dr. Kerry Campbell (Institute for Cancer Research, Philadelphia, PA). ELISA plate coating was performed as described above. However, following PBS washing, an additional blocking step was performed with PBS containing 5% BSA (Sigma-Aldrich) and 0.1% Tween-20 (U-CyTech) for 2 h at 37°C. Once blocked, plates were washed with PBS and incubated with heat-inactivated sera/plasma or IvIg for 2 h at 37°C. Plates were washed with PBS, and 2×10^5 GFP-CD16 (176V) NK-92 cells were added to each well and incubated at 37°C with 5% CO_2 for 5 h. Anti-human CD107a allophycocyanin (clone A4H3; BD Biosciences) and 1 mM EDTA were added to the cells for 30 min at room temperature in the dark. The GFP-CD16 (176V) NK-92 cells were washed twice with PBS, fixed with 1% formaldehyde, and acquired on an LSR II flow cytometer. Analysis was performed using FlowJo X software version 10.0.7r2 (TreeStar, Ashland, OR).

Data and statistical analysis. Statistical analysis was performed with GraphPad Prism version 6.05 (GraphPad, San Diego, CA). Binding data (Figs. 1–4) were fitted using Prism software, to log(agonist) versus response (variable slope, constraining bottom value = 0, the top value was allowed to vary freely). The 95% confidence interval (C.I.) for the individual fitted values for EC_{50} are indicated graphically for the representative curves in Fig. 1E and in the insets in Fig. 2B–E. Horizontal bars in Fig. 2B–E representing $EC_{20} - EC_{80}$ were calculated similarly. Cumulative data shown as EC_{50} with error bars are presented as mean ± 95% C.I. in Figs. 2F, 3K, and 3L. Curve fitting for some low-affinity interactions, with IgG2 and IgG4, were ambiguous, and EC_{50} values were only used from data fitting at $r^2 > 0.97$. When binding was undetectable or too weak to enable adequate fitting, the EC_{50} value was not calculated.

Binding to wild-type (WT) versus nonfucosylated IgG in Fig. 2F and, likewise, binding to dilutions of pre-2009 versus 2010 preparations of IvIg were evaluated by the Mann–Whitney unpaired *t* test. Data in Fig. 4 from five experiments were analyzed together by normalizing all OD values to the A450nm value for 250 μg/ml IvIg batch 1848–opsonized H3 HA bound by HRP-conjugated anti-IgG (normalized point denoted by § in Fig. 4). Similarly in Fig. 5A, 5B, and 5D, A450nm values were normalized using the A450nm value for 250 μg/ml IvIg batch 1848–opsonized H1 HA bound by dimeric rsFcγRIIIa Val^{158}. For Figs. 6 and 7, A450nm values were normalized to receptor binding to directly coated IvIg (5 μg/ml), and the pairs of assays were fitted by linear regression; data in Fig. 5D were fitted to log(agonist) versus response. Correlations were assessed by nonparametric Spearman analysis.

Results

Characterization of dimeric rsFcγRs using model human IgG1 ICs

The universal requirement for "near-neighbor" clustering of low-affinity FcRs by appropriately arrayed Fc portions in ICs underpins proinflammatory Ab-dependent effector functions. Because cell surface FcγRII and FcγRIII are low-affinity receptors for IgG that avidly bind ICs, we engineered genetic homodimers of their ectodomains, using a flexible linking sequence from the membrane proximal stalk, to generate defined probes that avidly bind to "near-neighbor" Ab pairs in ICs.

The biotin-labeled genetically fused dimeric ectodomains of FcγRIIa His^{131}, FcγRIIIa Val^{158}, and FcγRIIIa Phe^{158} were produced in cells expressing BirA ligase in the endoplasmic reticulum (46). The activities of these purified human dimeric rsFcγRs were initially characterized by testing their binding activities to different forms of model ICs formed with human IgG1 and TNP-BSA Ag or by capture with anti-$F(ab')_2$. Subnanomolar concentrations of the dimeric rsFcγRIIa and dimeric rsFcγRIIIa had detectable binding to both forms of IgG ICs, whereas the monomeric forms of the proteins had >1000-fold lower binding activity (Fig. 1). The weak binding of the receptor monomers (Fig. 1A) indicates that the avid binding of the receptor dimers requires pairs of Ab Fc regions that are presented with a proximity to each other that allows the simultaneous binding of the two receptor modules making up the dimeric rsFcγR. It is such "near-neighbor" IgGs that are required for activation of cells via engaging and clustering FcRs.

The dimeric rsFcγRIIa binding to ICs formed with anti-TNP IgG1 and TNP-BSA Ag gave an EC_{50} ~3-fold higher than for ICs formed by capture of IgG1 with plate-bound $F(ab')_2$ anti-human $F(ab')_2$ (Fig. 1B, 1E). Likewise, dimeric rsFcγRIIIa Phe^{158} had higher binding activity to the TNP-BSA:IgG ICs than to the anti-human $F(ab')_2$:IgG complexes (EC_{50}, 250 pM and 1.4 nM, respectively, Fig. 1D, 1E), whereas this trend was not apparent with the higher-affinity Val^{158} allelic form of dimeric rsFcγRIIIa (EC_{50}, 46 and 48 pM, respectively) (Fig. 1C, 1E).

Dimeric rsFcγR binding detects the modified FcγR-binding activity of Fc variants

The dimeric rsFcγR assays were further validated by analyzing the interactions of activating and inactivating variants of IgG1. Mutation of the lower hinge of IgG1, LL(234–235)AA (LALA mutant), greatly diminishes FcγR binding activity and FcR mediated–function (56, 57). The loss of binding activity was recapitulated in the dimeric rsFcγR assays, with dimeric rsFcγRIIa and dimeric rsFcγRIIIa binding only weakly to IgG1-LALA ICs (Fig. 2B–E). In contrast, enhanced binding of dimeric rsFcγRIIIa to afucosyl IgG1 (58) was demonstrated with the receptor dimer assay (Fig. 2D, 2E). Both the higher-affinity (Val^{158}, $p = 0.008$) and the lower-affinity (Phe^{158}, $p = 0.016$) allelic forms of the receptor had significantly increased affinity to the nonfucosyl IgG (Fig. 2D–F). For dimeric rsFcγRIIIa Val^{158}, the EC_{50} decreased from 118 ng/ml (86–150, 95% C.I.) with WT IgG to 43 ng/ml (21–65, 95% C.I.) with nonfucosyl IgG; likewise for the Phe^{158} allele, the EC_{50} decreased from 275 ng/ml (89–460, 95% C.I.) to 97 ng/ml (55– 139, 95% C.I.). Thus, the dimeric rsFcγR assays are useful for discriminating variants of IgG with enhanced or diminished FcR activity.

IC formation measured by determining the bound IgG with anti-human IgG had a broad response profile, with the 20–80% response occurring over an 18-fold increase in IgG concentration (i.e., Fig. 2A, open bar; anti-IgG, EC_{20}–EC_{80} for WT IgG1 = 8–151 ng/ml). In contrast, a distinctive feature of the dimeric rsFcγR binding activity was a narrow response profile, with the 20–80% response occurring over a 2–3-fold increase in IgG concentration (i.e., Fig. 2B, open bar; FcγRIIa H131, EC_{20}–EC_{80}; WT IgG1 = 150–360 ng/ml). The steeper character of these dimeric rsFcγR response curves can also be described by the numerical equivalent of the Hill constant (Table I). Although anti-IgG binding is typically described by a coefficient near or <1, the binding curves in Fig. 2 are typical of dimeric rsFcγR profiles for binding to IgG1 ICs with coefficients, in this case, ranging from 2.3 to 4.1 (Table I). The steeper receptor-binding curves reflect the requirement for closely placed "near-neighbor" IgG-Fcs for dimeric rsFcγR binding, which produces a response over a narrow range of IgG concentration that would not be

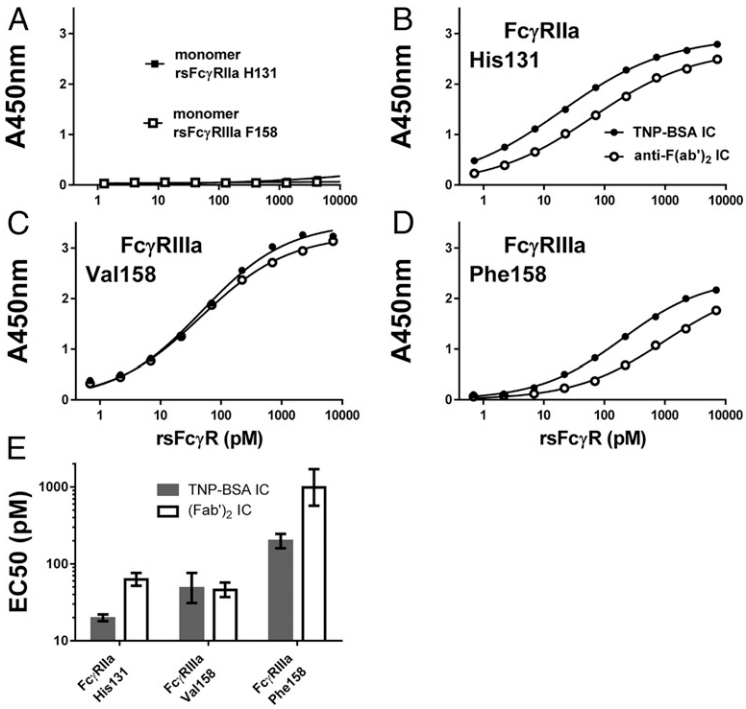

FIGURE 1. Biotin-labeled dimeric rsFcγRs selectively bind to IgG1 ICs. Human IgG1 (1 μg/ml) was formed into ICs by binding to TNP-BSA (**A**–**D**) or by capture with plate-bound $F(ab')_2$ fragments of anti-human $F(ab')_2$ (B–D). These ICs were then reacted with monomeric rsFcγRIIa His^{131} or monomeric rsFcγRIIIa Phe^{158} (A), dimeric rsFcγRIIa His^{131} (B), dimeric rsFcγRIIIa Val^{158} (C), or dimeric rsFcγRIIIa Phe^{158} with subsequent detection with streptavidin-HRP (D). (**E**) Data were fitted using Prism software to log(agonist) versus response (variable slope, constraining bottom value = 0). EC_{50} values from fitted curves are shown with 95% C.I.

obvious from measuring Ab binding or titer (e.g., compare Fig. 2A with Fig. 2B–E).

Dimeric rsFcγR binding is determined by IgG subclass and presentation of the Fc

The effect of IgG subclass on dimeric rsFcγR binding was investigated using two established methods of forming model ICs (37, 38). First, the capture of IgG by the $F(ab')_2$ anti-human $F(ab')_2$ to form ICs (Fig. 3A) results in the presentation of Fc regions of the IgGs in varied orientations for dimeric rsFcγR binding (Fig. 3C, 3E, 3G, 3I). Second, TNP hapten-specific rIgG and TNP-BSA form ICs (Fig. 3B) in which all IgGs are oriented by the same variable domain:hapten interaction and thus, display a more uniform presentation of Fcs for dimeric rsFcγR binding (Fig. 3D, 3F, 3H, 3J).

Dimeric rsFcγRIIa His^{131} binding to human IgG1, IgG2, IgG3, or IgG4 captured using $F(ab')_2$ anti-human $F(ab')_2$ to form ICs

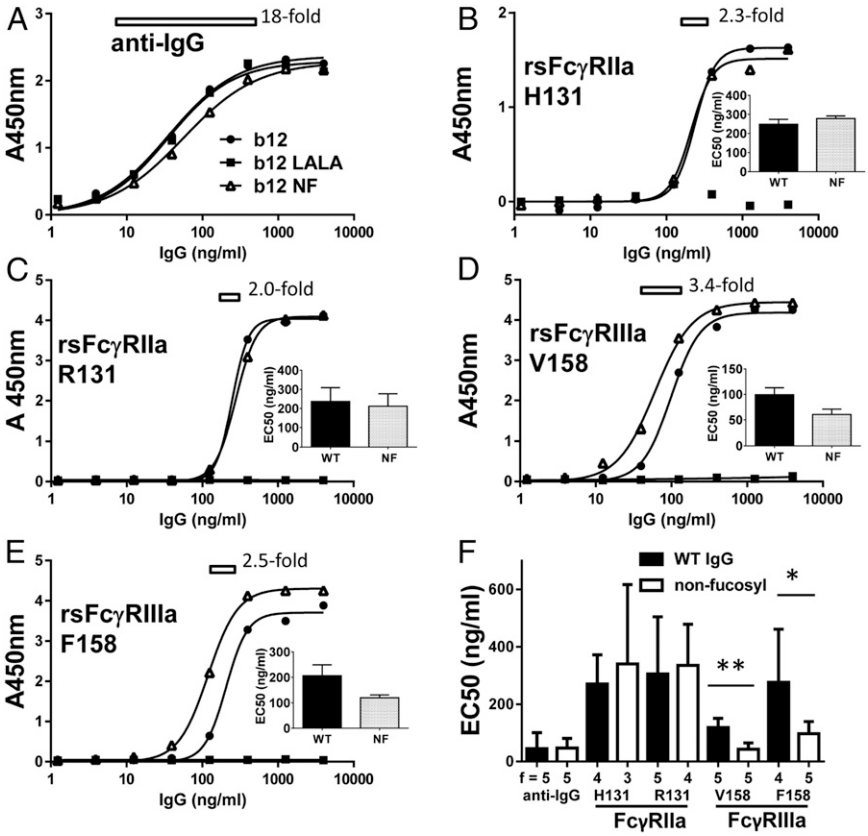

FIGURE 2. Characterization of normal and variant IgG1 with dimeric rsFcγR assay. Normal IgG1, nonfucosyl IgG1, and LALA mutant IgG1 were captured using $F(ab')_2$ fragment of anti-human $F(ab')_2$ to form ICs and reacted with HRP-conjugated anti-human IgG (**A**) or the following human dimeric rsFcγR: FcγRIIa His^{131} (**B**), FcγRIIa Arg^{131} (**C**), FcγRIIIa Val^{158} (**D**), or FcγRIIIa Phe^{158} (**E**). Data were fitted using Prism software to log(agonist) versus response (variable slope, constraining bottom value = 0). Individual fitted values for EC_{50} ± 95% C.I. are shown as insets in (B)–(E). (**F**) EC_{50} values ± 95% C.I. were evaluated by the Mann–Whitney *t* test. The EC_{20}–EC_{80} ranges for binding to WT IgG1 were also derived from the curve fitting and are shown as horizontal open bars annotated with the fold ratio of EC_{80}/EC_{20} in (A)–(E). $*p \leq 0.05$, $**p \leq 0.01$. f, number of curve fits from independent experiments.

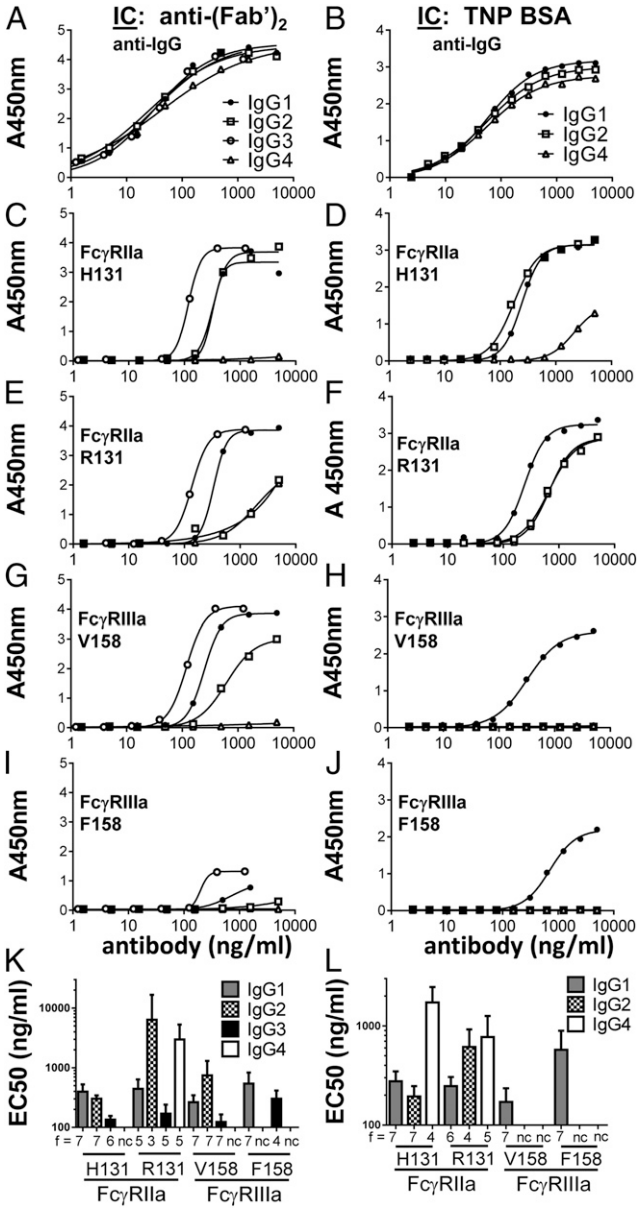

FIGURE 3. Dimeric rsFcγRIIa and rsFcγRIIIa selectively bind IgG subclass ICs, and binding is affected by the manner of IC formation. Human IgG subclasses at concentrations from 500 to 1 ng/ml were formed into ICs by capture of myeloma IgG1, IgG2, IgG3, or IgG4 proteins with plate-bound $F(ab')_2$ fragment of anti-human $F(ab')_2$ (**A**, **C**, **E**, **G**, and **I**) or by recombinant human IgG1, IgG2, and IgG4 subclass Abs specific for the hapten TNP binding to TNP-BSA (**B**, **D**, **F**, **H**, and **J**). These ICs were then reacted with HRP-conjugated anti-human IgG (A and B) or with the following dimeric rsFcγR: FcγRIIa His^{131} (C and D), FcγRIIa Arg^{131} (E and F), FcγRIIIa Val^{158} (G and H) or FcγRIIIa Phe^{158} (I and J) with subsequent detection with streptavidin-HRP. Mean EC_{50} values ± 95% C.I. (**K** and **L**). f, number of curve fits from independent experiments; nc, not calculated.

was strongest to IgG3 complexes, was equivalent between IgG1 and IgG2, and was least strong to IgG4, for which a binding curve could not be fitted unambiguously (i.e., IgG3 > IgG1 ~ IgG2 >> IgG4, Fig. 3C). Across experiments, the EC_{50} values for dimeric rsFcγRIIa His^{131} binding to Ab pairs within ICs formed with IgG1, IgG2, and IgG3 were defined by 95% C.I.s of 270–520, 260–340, and 110–160 ng/ml (means of 400, 300, and 130 ng/ml, respectively, Fig. 3K). Likewise, the dimeric rsFcγRIIa Arg^{131} bound strongly to IgG3 and IgG1 IC, mean EC_{50} = 440 and 170 ng/ml, respectively (Fig. 3E, 3K), but weakly to IgG2, in contrast to the His^{131} receptor, and IgG4, mean EC_{50} = ~ 6 and 3 μg/ml, respectively (Fig. 3E, 3K). This hierarchy of binding defined in the receptor dimer assay (Fig. 3K, Table II) is comparable to the reported reactivity of the allelic forms of FcγRIIa as a cell surface receptor (34, 37, 38).

The nature of the IC also influenced dimeric rsFcγR binding. The binding differed most markedly for the weakest FcR interactions observed. For example, dimeric rsFcγRIIa His^{131} binding activity was just detectable with ICs formed with anti-human $F(ab')_2$ at 5 μg/ml IgG4 (Fig. 3C), whereas when binding to IC of IgG4 formed with the Ag TNP-BSA, the signal was ~6-fold higher at 5 μg/ml IgG4 (Fig. 3D, 3L, EC_{50} ~ 2 μg/ml). For this lowest-affinity FcR interaction, Ab presentation in these different forms of ICs profoundly affects receptor binding. For the higher-affinity interactions, differences between the two methods of IC formation for FcγR binding were less apparent. For example, the dimeric rsFcγRIIa His^{131} bound similarly to the anti-human $F(ab')_2$:IgG1 and IgG2 ICs (EC_{50} = 400 and 300 ng/ml respectively, Fig. 3C, 3K) and to the TNP-BSA:IgG1 and IgG2 ICs (EC_{50} = 280 and 190 ng/ml, respectively, Fig. 3D, 3L).

The dimeric rsFcγRIIa Arg^{131} bound anti-human $F(ab')_2$ ICs with the ranking IgG3 > IgG1 >> IgG2 ~ IgG4 (Fig. 3E); a similar hierarchy (IgG1 > IgG2 ~ IgG4) was apparent with anti-TNP ICs (Fig. 3F, Table II). Thus, the allelic forms of dimeric rsFcγRIIa recapitulate the IgG subclass binding behavior of their cellular counterparts, and their weak binding to IgG4 is influenced by Fc presentation in different forms of ICs.

Analysis of the allelic variants of dimeric rsFcγRIIIa proteins showed, as expected, that the dimeric rsFcγRIIIa Val^{158} had greater binding activity to IgG1 IC than the lower-affinity dimeric rsFcγRIIIa Phe^{158} (EC_{50} = 260 versus 540 ng/ml Fig. 3K; EC_{50} = 170 versus 570 ng/ml, Fig. 3L). The hierarchies of binding to anti-$F(ab')_2$: ICs (IgG3 > IgG1 > IgG2 >> IgG4) and TNP-BSA ICs (IgG1 >>> IgG2, IgG4 = nil) (Fig. 3G–L, Table II) were largely comparable to the binding of ICs of the different IgG subclasses to cell surface–expressed FcγRIIIa (34, 37, 38).

It is notable that, in this study (Fig. 3) and in other studies (37, 38), differences occur in FcγR binding to ICs made with anti-$F(ab')_2$ or TNP-BSA Ag (Table II). Using the assay to evaluate FcγRIIIa interactions with anti-TNP ICs revealed, similarly to FcγRIIa, that the weakest interactions between dimeric rsFcγRIIIa and ligand were influenced the most by the manner of formation of the IC. The interactions of ICs of IgG2 and IgG4 with the higher-affinity (Fig. 3G, 3H) and lower-affinity (Fig. 3I, 3J) alleles of the dimeric rsFcγRIIIa were undetectable with the anti-TNP–formed ICs (Fig. 3H, 3J), but binding was measurable for ICs of $F(ab')_2$ anti-human $F(ab')_2$, with IgG2 binding the dimeric rsFcγRIIIa Val^{158} (Fig. 3G, EC_{50} = 620, 95% C.I. = 520–740 ng/ml). Clearly, the binding, or nonbinding, to IgG subclasses by FcγRIIa (compare IgG4 IC binding in Fig. 3C and Fig. 3D) and FcγRIIIa (compare IgG2 IC binding in Fig. 3H and Fig. 3G) can depend on the manner of incorporation of IgG into the IC.

In summary, the dimeric rsFcγRs demonstrate binding equivalent to cell surface FcγRs with regard to the hierarchy of binding to IgG subclasses, e.g., binding to IgG3 > other subclasses, (see figure 2A in Ref. 37); the subclass specificity of the polymorphic forms of FcγR (e.g., binding of IgG2 by FcγRIIa His^{131} > FcγRIIa Arg^{131}); the expected differences in binding strength of the polymorphic forms of FcγR (e.g., FcγRIIIa Val^{158} > FcγRIIIa Phe^{158}); and the appropriately altered binding of LALA hinge mutant and nonfucosyl-variant IgG, b12. In addition, how the Fc is presented influences dimeric rsFcγR binding, especially for low-affinity interactions, in particular IgG2 and IgG4 [e.g., FcγRIIa His^{131} with IgG4 ICs (Fig. 3C, 3D) and FcγRIIIa with IgG2 (Fig. 3G–J)].

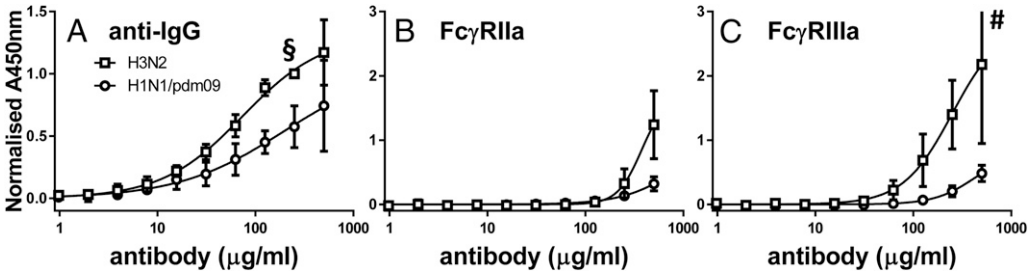

FIGURE 4. Dimeric rsFcγR binding to IvIg-opsonized influenza A HA occurs only at high levels of bound IgG. Influenza HA of A(H1N1)pdm09 (A/California/04/2009 (H1N1) or A/Perth/16/2009 (H3N2) was coated onto plates and opsonized with the indicated concentrations of IvIg (1848-2010). Binding to the opsonized H1 and H3 Ags is shown for anti-IgG HRP (**A**), dimeric rsFcγRIIa His^{131} (**B**), and dimeric rsFcγRIIIa Val^{158} (**C**). The OD value for anti-IgG binding at 250 μg/ml of IvIg binding to H3 (§) was used to normalize ODs for each independent experiment (n = 5). A clipped 95% C.I. error bar is denoted by the pound sign (#).

The use of dimeric rsFcγRs in the analysis of anti-influenza A immunity: dimeric rsFcγR binding to serum IgG–opsonized influenza HA

There is increasing evidence that Fc-mediated functions are important in clearance of influenza infections (6, 12), but typical assays to measure such responses through activation of cells or killing of target cells remain cumbersome. The dimeric rsFcγR-binding assay was evaluated in the context of Abs to this common viral pathogen. Dimeric rsFcγR-binding activity to ICs formed between influenza A HA and human IgG Abs was assessed using IvIg and HA from the 2009 H1N1 pandemic virus and from an H3N2 virus. Because IvIg is prepared from the sera of thousands of individuals, it is composed of the IgG Ab repertoire at a population level and opsonizes all epitopes of HA for which specific IgG molecules exist in the population. Like the model ICs (Figs. 2, 3), H3N2 HA opsonized with IvIg (Fig. 4) showed a steeper dimeric rsFcγR-binding profile (Fig. 4B, 4C) compared with the broader profile for the detection of opsonizing IgG (anti-IgG, EC_{20}–EC_{80} = 20–275 μg/ml, Fig. 4A). The estimated EC_{50} values for dimeric rsFcγR binding (rsFcγRIIa His^{131} EC_{50}^{H3} ~ 370 μg/ml; FcγRIIIa Val^{158} EC_{50}^{H3} ~ 250 μg/ml) were several fold above the EC_{50} for IgG binding (anti-IgG EC_{50}^{H3} = 74 μg/ml), a feature also consistent with the model ICs. Enumeration of the EC_{50} values for dimeric rsFcγR binding could only be approximated by curve fitting because the binding did not reach saturation (r^2 = 0.88–0.92, Fig. 4B, 4C). The same trends were apparent in dimeric rsFcγRIIa and dimeric rsFcγRIIIa binding to ICs formed by IvIg opsonization of A (H1N1)pdm09 HA, although the levels of opsonization and dimeric rsFcγR binding were less than for the HA from H3N2 A/Perth/16/2009 (Fig. 4B, 4C). For input concentrations of IvIg < 100 μg/ml, opsonization of HA by IgG, although well detected by anti-IgG, is sparse and therefore, bound IgGs cannot simultaneously engage the two FcγR-binding modules of the dimeric rsFcγRIIa or dimeric rsFcγRIIIa. The relatively steep reaction profiles of the dimeric rsFcγR-binding curves dictate that, rather than determining end point titer, a meaningful measure of the FcR activity for comparing different sera is the dimeric rsFcγR-binding signal at a fixed Ab concentration (or plasma/serum dilution) within the EC_{20}–EC_{80} range of the assay.

FcR activity of IvIg-opsonized H1N1 pandemic HA mirrors HA-inhibition activity

Fc-mediated functional responses to the HA of novel influenza A strains entering the population, such as the 2009 swine influenza. A(H1N1)pdm09 (A/California/04/2009) exist, pre-exposure via cross-reactive Abs. Upon exposure via infection or vaccination, strain-specific HA inhibition titers are increased, and Fc-mediated

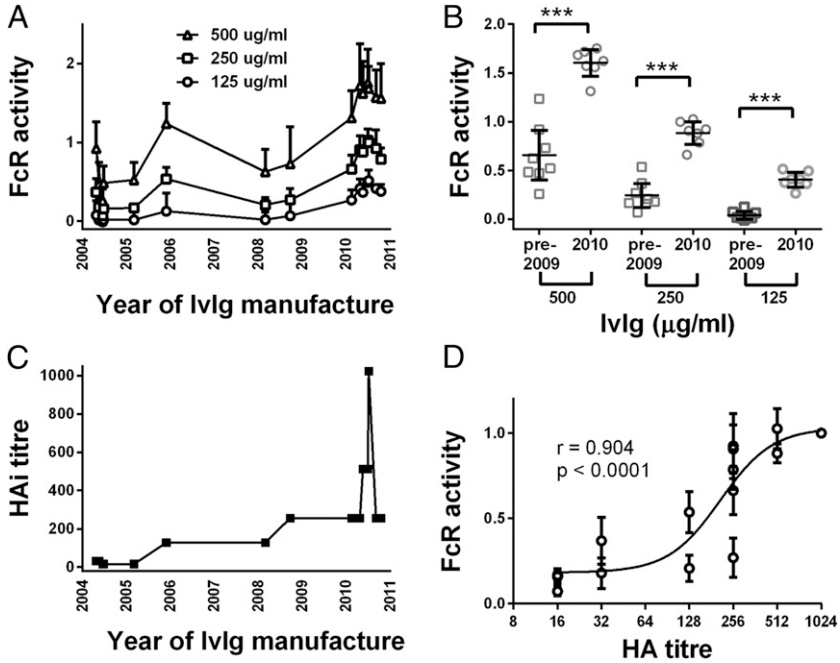

FIGURE 5. Dimeric rsFcγRIIIa binding to ICs of IvIg-opsonized HA of A(H1N1)pdm09 virus correlates with HA-inhibition titer, peaking with IvIg prepared in 2010. Fifteen commercial IvIg preparations (prepared in 2004–2010) were diluted to 500, 250, and 125 μg/ml (n = 4, 5, and 4 experiments, respectively) and used to opsonize influenza HA from A(H1N1) pdm09 virus. The dimeric rsFcγRIIIa Val^{158} binding activity of these ICs was determined and analyzed across experiments by normalizing A450nm values to that for IvIg 1848 at 250 μg/ml. (**A**) Dimeric rsFcγRIIIa Val^{158} binding activity (means for the eight pre-2009 and seven 2010 IvIg preparations) was compared using an unpaired Mann–Whitney t test, ***$p \leq 0.001$ (**B**). HA-inhibition titer for the IvIg preparations (from table I in Ref. 54) (**C**) and the correlation between FcR activity and HA-inhibition titer (**D**). The values were correlated using nonparametric Spearman analysis.

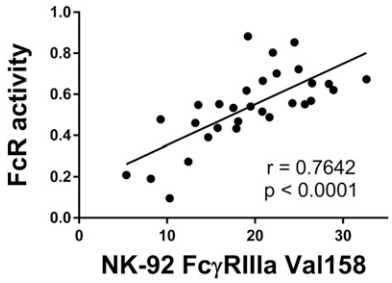

FIGURE 6. The dimeric rsFcγRIIIa Val^{158} assay correlates with NK-92-FcγRIIIa Val^{158} activation by influenza A HA, A/Perth/16/2009 (H3N2). ICs were formed by reacting plasma from 30 individuals with plate-bound HA A/Perth/16/2009 (H3N2). ICs formed with plasmas diluted at 1:80 were assessed for the binding of dimeric rsFcγRIIIa Val^{158} and compared with ICs formed with plasmas diluted at 1:40 for the capacity to activate NK-92 cells expressing FcγRIIIa Val^{158}. Dimeric rsFcγRIIIa Val^{158} binding was normalized using binding in wells directly coated with IvIg (5 μg/ml). The two assays were correlated using nonparametric Spearman analysis and fitted by linear regression.

functional activity toward virally infected cells also increases. Furthermore, NK cell–activating capacity of HA Abs trended toward an increase in pooled IgG preparations after the 2009 H1N1 influenza pandemic (54). Therefore, we assessed whether the dimeric rsFcγR assay was capable of detecting subtle changes in the FcR activity of HA Abs at the population level, as represented in pooled IgG (IvIg), after the 2009 H1N1 pandemic. Thus, IvIg was used to opsonize H1N1 pandemic HA, and dimeric rsFcγRIIIa binding was measured. IvIg preparations during 2010 showed higher dimeric rsFcγRIIIa-binding activity, suggesting that the FcR-activating capacity of Abs specific for the HA of influenza virus A(H1N1)pdm09 was increased subsequent to the emergence of the pandemic in 2009 (Fig. 5A). Interestingly, this increased dimeric rsFcγRIIIa activity appeared to be transient, peaking and declining in 2010. When the dimeric rsFcγRIIIa activity was compared pre-2009 with 2010, the postpandemic increase in receptor activity was significant ($p = 0.0003$) over the three Ab concentrations tested (Fig. 5B). Consistent with the dimeric rsFcγR assay being a measure of a correlate of immunity, the peak in FcγR activity in 2010 was mirrored by a contemporaneous peak in HA-inhibition titer (Fig. 5C). The correlation between these differing, but contemporaneous, Ab functions (Fig. 5D, $p < 0.0001$) suggests a biological relevance for the dimeric rsFcγR assay and lends support to the idea of coordination of Ab functions in immunity.

Dimeric rsFcγR binding is a predictor of NK cell activation

Next, the relationship between dimeric rsFcγR binding and cellular FcγR effector function was investigated. The ability of dimeric rsFcγR activity to correlate with cellular activation by HA-specific Abs was tested by comparison with the activation of NK-92 cells expressing FcγRIIIa Val^{158}, a well-established system for measuring Ab-mediated NK activation. Plasma from individuals was used to separately opsonize HA of Perth (H3N2) and to activate NK-92-FcγRIIIa Val^{158} cells and for binding dimeric rsFcγRIIIa Val^{158}. The cell and dimeric rsFcγRIIIa activities correlated strongly ($p < 0.0001$), validating use of the dimeric rsFcγRIIIa receptor to predict cellular responses (Fig. 6). Thus, the FcR dimer assay ranks individuals on the basis of the NK cell–activating potential of their anti-HA IgG Abs. Next, the ability of the dimeric rsFcγR assay to predict the capacity of anti-HA ICs to activate fresh blood primary NK cells was assessed. The plasma from 30 individuals was used to opsonize A(H1N1)pdm09 HA, and these ICs were used to activate NK cells and bind dimeric rsFcγR (Fig. 7). NK cell activation (intracellular IFN-γ and/or CD107a surface expression) correlated more strongly with binding of the dimeric rsFcγRIIIa Val^{158} ($p = 0.005$, Fig. 7C) than the anti-HA IgG Ab titer ($p = 0.027$, Fig. 7A) or Ab EC_{50} ($p = 0.79$, Fig. 7B). Thus, dimeric rsFcγRIIIa binding activity to IgG-opsonized HA correlates with IC capacity for NK activation.

Discussion

FcγRs and IgG Abs are increasingly understood to play key roles in immunity to pathogens, vaccine responses, and autoimmunity. Although many effector functions can result from FcγR activation, all are triggered when multiple Fc regions of IgGs in ICs bind and cluster receptors to initiate signaling (59, 60). To identify IgG molecules that bind to Ag and are sufficiently closely spaced to bind and cluster FcγRs, we produced defined dimeric soluble forms of FcγRIIa and FcγRIIIa as mimics of neighboring, signaling FcγRs on the cell surface. The usefulness of these probes was tested using IgG ICs formed with model Ags and with human Abs to influenza HA.

A general feature of the assay was a higher threshold and steeper reaction profile for dimeric rsFcγR binding to IC than the binding of anti-IgG. This follows from the requirement for divalent binding of the dimeric rsFcγR by bridging the closely spaced Fcs of neighboring Abs. At IgG concentrations above the EC_{50} for opsonization, relatively small differences in the levels of opsonizing IgG presumably achieve a critical density of presented Fc regions that result in large increases in dimeric rsFcγR-binding activity.

The use of the dimeric rsFcγR assays demonstrated expected hierarchies of IgG subclass binding IgG3 > IgG1 ~ IgG2 >> IgG4 for FcγRIIa (His^{131}) interactions and IgG3 > IgG1 >> IgG2 ~ IgG4 for FcγRIIa (Arg^{131}) interactions (Fig. 3, Table II), which were comparable to the reported activities of the cell surface FcγRs (34, 37, 38); the FcγRIIIa Phe^{158} allele has weaker binding activity than the Val^{158} allelic form, and both FcγRIIIa Val^{158} and FcγRIIIa

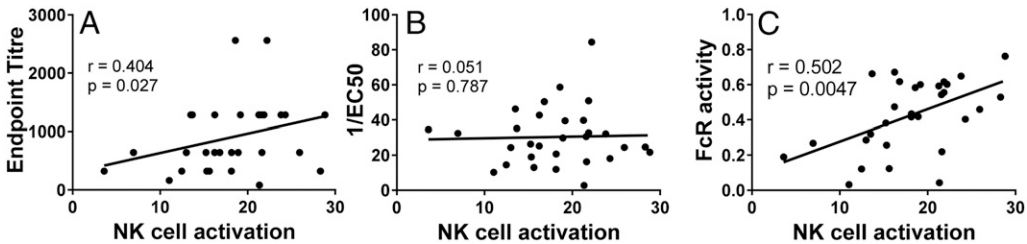

FIGURE 7. Dimeric rsFcγR binding has superior correlation with donor NK activation by influenza A HA, A(H1N1)pdm09 than with anti-IgG end point titer or EC_{50}. ICs were formed by reacting plasma from 30 individuals with plate-bound HA from A(H1N1) pdm09 virus. Activation of the CD56$^+$ NK cell population of PBMCs by these ICs was measured by intracellular stain for IFN-γ and/or surface expression of CD107a and was correlated with IgG end point titer (**A**), IgG 1/EC_{50} (**B**), and dimeric FcγRIIIa Val^{158} binding, normalized using binding in wells directly coated with IvIg (5 μg/ml) (**C**). Each pair of assays was correlated using nonparametric Spearman analysis and fitted by linear regression.

Table I. Shape "H" coefficients from IC-binding curves

Figure	Probe	H[a]	95% C.I.
Fig. 2A	Anti-IgG (opsonization)	1.0	0.67–1.2
Fig. 2B	Dimeric rsFcγRIIa His^{131}	3.3	1.8–4.7
Fig. 2C	Dimeric rsFcγRIIa Arg^{131}	4.1	3.3–4.8
Fig. 2D	Dimeric rsFcγRIIIa Val^{158}	2.3	1.7–2.9
Fig. 2E	Dimeric rsFcγRIIIa Phe^{158}	3.1	2.1–4.1

[a]H is a descriptor of steepness of the response curve numerically equivalent to the Hill coefficient.

Phe^{158} showed the expected higher binding activity to afucosylated IgG1; FcγRIIa and FcγRIIIa binding to the weaker interacting subclasses, IgG2 and IgG4, was affected by the nature of the IC; dimeric rsFcγR-binding activity to IgG-opsonized Ag showed a higher threshold and steeper reaction profile than the binding of anti-IgG; as expected, receptors failed to bind to IgG1 containing the established FcR binding–inactivation LALA lower hinge mutant; and dimeric rsFcγRIIIa binding activity of ICs correlated with NK activity measured using FcγRIIIa-expressing NK-92 cells or primary NK cells and detected a transient increase in the activity of anti-H1pdm HA Abs in IvIg prepared during 2010 postpandemic H1N1 influenza. This last finding demonstrated that the dimeric rsFcγR assay was at least as capable as cell-based assays (54) in revealing changes in Ab activity.

The strength of engagement of FcγRs by IgG depends on Fc-intrinsic properties, such as amino acid residues at the interaction interfaces and glycosylation, but it also depends on how an Ab reacts with Ag to form an IC or opsonized target. Interestingly, the subclasses IgG2 and IgG4, which have weaker interactions with FcγRs, exhibited different FcγRIIa- and FcγRIIIa-binding activities when oriented by capture with anti-F(ab′)$_2$ compared with when they were bound by TNP-BSA Ag. Both of these methods of forming ICs are described in studies that defined cellular FcγR interactions and the effect of IC size on these interactions (37, 38). FcγRII and FcγRIII binding to Fc are low-affinity interactions for which the 1:1 intrinsic FcR:Fc reactions have been well described. However, the biological interactions of FcγRII and FcγRIII with ICs are multivalent and even with the divalent interactions described in this article, the net outcome of weak but avid binding reactions was profoundly affected by differences in ligand presentation in the IC. This phenomenon is important in evaluating the activities of therapeutic Abs, particularly agonist mAbs (61), developed in low FcR-binding formats, such as IgG2 or IgG4 backbones. Thus, although the Fc-intrinsic effects can be engineered by altering amino acid residues and glycosylation, the consequences of opsonization-related effects are difficult to predict because Abs are highly diverse, with ~10^{11} possible Ab:Ag interactions (62).

The dimeric rsFcγR assay described in this article has a number of advantageous features. Dimeric rsFcγRs are genetically defined dimers, have site-specific biotinylation, and, importantly, bind ligand without further complexing (e.g., to streptavidin) to provide multivalency. The intrinsic FcγRIIa and FcγRIIIa interactions with IgG are 1:1 and were thoroughly characterized by surface plasmon resonance assays (e.g., BIAcore, figure 3 in Ref. 37), but biological responses mediated by these receptors result from multivalent interactions. The assay of the dimeric receptor interaction with two Fcs described in this article is a measure of the minimal avid interaction of IgG with the low-affinity FcγRs. The dimeric rsFcγR binds to adjacent Fcs when presented by two Abs in close proximity. The correlation of receptor activity assayed off the cell membrane with activity in a cellular context, and indeed with in vivo biology, is difficult to evaluate. Nonetheless, it can be noted that other cell-free approaches, which clearly produced key insights (20, 63–66), require receptor complexing or immobilization resulting in measuring higher or ill-defined valency interactions, respectively. In contrast, dimeric FcγR binding measures the spatial relationship of pairs of Abs complexed with Ag, with the effects of receptor polymorphism, Ab subclass, and glycosylation contributing to the overall measure of FcγR activity.

Furthermore, the use of FcγR dimers is informative and does not require specialized equipment. It needs only limited amounts of sample and can be used to evaluate the FcγR activities of many types of IgG Abs bound to different Ags. Central to the assay is the biotinylated dimer rsFcγR, which could be easily incorporated into powerful, parallel high-throughput bead-based assays (20, 63, 64, 66–68), adapting these for detecting closely spaced Ab pairs.

Evaluating the quality of IgG responses for FcγR activation will be of particular importance for understanding natural (67) and vaccine-induced immunity (6, 18, 20, 24, 69) to viruses and other infectious diseases. The detection of a transient increase in the activity of IvIg from 2010 toward H1N1 pandemic HA, which correlated with HA-inhibition titer and NK activation, indicates that the dimeric rsFcγR assay may provide a useful measure of immunity. Moreover, dimeric rsFcγR may be of value for evaluating therapeutic IgG and IgG mixtures. Therapeutic IgG Abs have revolutionized the treatment of some cancers and rheumatoid arthritis; however, the application of therapeutic Abs to infectious disease may be more challenging in situations in which strain differences and a need for sterilizing immunity may necessitate the use of Ab cocktails of increasing complexity and functionality (70, 71). Indeed, such cocktails of Abs are used for treatment of rabies virus (72), toxins (73), and, most recently, Ebola (74). The

Table II. Reactivity of dimeric rsFcγRs with IgG ICs

Dimeric rsFcγR	IC Format	Binding Hierarchy						
FcγRIIa His^{131}								
Fig. 3C	Anti-F(ab′)$_2$	IgG3	>	IgG1	~	IgG2	>>	IgG4
Fig. 3D	TNP-BSA			IgG1	≥	IgG2	>>	IgG4
FcγRIIa Arg^{131}								
Fig. 3E	Anti-F(ab′)$_2$	IgG3	>	IgG1	>>	IgG2	~	IgG4
Fig. 3F	TNP-BSA			IgG1	>	IgG2	~	IgG4
FcγRIIIa Val^{158}								
Fig. 3G	Anti-F(ab′)$_2$	IgG3	>	IgG1	>	IgG2	>>	IgG4
Fig. 3H	TNP-BSA			IgG1	>>>	IgG2, IgG4 = nil		
FcγRIIIa Phe^{158}								
Fig. 3I	Anti-F(ab′)$_2$	IgG3	>	IgG1	>	IgG2	>>	IgG4
Fig. 3J	TNP-BSA			IgG1	>>>	IgG2, IgG4 = nil		

Binding hierarchy for dimeric rsFcγR derived from Fig. 3.

FcR-activating activity of such mixtures of Abs is generally greater than for single therapeutic Abs, except in situations in which the target Ags are highly abundant (such as CD20 on B cell tumors) or have repeating epitopes.

The engineered FcγR ectodomain dimers described in this article measure the content of closely spaced, and thus, receptor-aggregating, pairs of "near-neighbor" IgG Abs on opsonized targets. Clearly, they are important tools for the prediction of FcγR activation by Ag-specific IgG and thereby, the evaluation of Ab responses to vaccines, infections, and therapeutic Abs.

Acknowledgments

We thank Dr. Amanda Gavin and Dr. Freya Fowlkes for helpful discussions, James Munro for technical assistance, Halina Trist for reading the manuscript, and Steven Rockman (bioCSL Ltd., Parkville, VIC, Australia) for supplying IvIg preparations.

Disclosures

The authors have no financial conflicts of interest.

References

1. Pollara, J., M. Bonsignori, M. A. Moody, M. Pazgier, B. F. Haynes, and G. Ferrari. 2013. Epitope specificity of human immunodeficiency virus-1 antibody dependent cellular cytotoxicity [ADCC] responses. *Curr. HIV Res.* 11: 378–387.
2. Kohl, S. 1991. Role of antibody-dependent cellular cytotoxicity in defense against herpes simplex virus infections. *Rev. Infect. Dis.* 13: 108–114.
3. Hashimoto, G., P. F. Wright, and D. T. Karzon. 1983. Antibody-dependent cell-mediated cytotoxicity against influenza virus-infected cells. *J. Infect. Dis.* 148: 785–794.
4. Petro, C., P. A. González, N. Cheshenko, T. Jandl, N. Khajoueinejad, A. Bénard, M. Sengupta, B. C. Herold, and W. R. Jacobs. 2015. Herpes simplex type 2 virus deleted in glycoprotein D protects against vaginal, skin and neural disease. *eLife* 4: 4.
5. Kramski, M., M. S. Parsons, I. Stratov, and S. J. Kent. 2013. HIV-specific antibody immunity mediated through NK cells and monocytes. *Curr. HIV Res.* 11: 388–406.
6. Jegaskanda, S., P. C. Reading, and S. J. Kent. 2014. Influenza-specific antibody-dependent cellular cytotoxicity: toward a universal influenza vaccine. *J. Immunol.* 193: 469–475.
7. Jegaskanda, S., J. T. Weinfurter, T. C. Friedrich, and S. J. Kent. 2013. Antibody-dependent cellular cytotoxicity is associated with control of pandemic H1N1 influenza virus infection of macaques. *J. Virol.* 87: 5512–5522.
8. Hessell, A. J., L. Hangartner, M. Hunter, C. E. Havenith, F. J. Beurskens, J. M. Bakker, C. M. Lanigan, G. Landucci, D. N. Forthal, P. W. Parren, et al. 2007. Fc receptor but not complement binding is important in antibody protection against HIV. *Nature* 449: 101–104.
9. Bournazos, S., F. Klein, J. Pietzsch, M. S. Seaman, M. C. Nussenzweig, and J. V. Ravetch. 2014. Broadly neutralizing anti-HIV-1 antibodies require Fc effector functions for in vivo activity. *Cell* 158: 1243–1253.
10. Bonsignori, M., J. Pollara, M. A. Moody, M. D. Alpert, X. Chen, K. K. Hwang, P. B. Gilbert, Y. Huang, T. C. Gurley, D. M. Kozink, et al. 2012. Antibody-dependent cellular cytotoxicity-mediating antibodies from an HIV-1 vaccine efficacy trial target multiple epitopes and preferentially use the VH1 gene family. *J. Virol.* 86: 11521–11532.
11. Bialuk, I., S. Whitney, V. Andresen, R. H. Florese, J. Nacsa, V. Cecchinato, V. W. Valeri, J. M. Heraud, S. Gordon, R. W. Parks, et al. 2011. Vaccine induced antibodies to the first variable loop of human immunodeficiency virus type 1 gp120, mediate antibody-dependent virus inhibition in macaques. *Vaccine* 30: 78–94.
12. DiLillo, D. J., G. S. Tan, P. Palese, and J. V. Ravetch. 2014. Broadly neutralizing hemagglutinin stalk-specific antibodies require FcγR interactions for protection against influenza virus in vivo. *Nat. Med.* 20: 143–151.
13. Throsby, M., E. van den Brink, M. Jongeneelen, L. L. Poon, P. Alard, L. Cornelissen, A. Bakker, F. Cox, E. van Deventer, Y. Guan, et al. 2008. Heterosubtypic neutralizing monoclonal antibodies cross-protective against H5N1 and H1N1 recovered from human IgM+ memory B cells. *PLoS One* 3: e3942.
14. Impagliazzo, A., F. Milder, H. Kuipers, M. V. Wagner, X. Zhu, R. M. Hoffman, R. van Meersbergen, J. Huizingh, P. Wanningen, J. Verspuij, et al. 2015. A stable trimeric influenza hemagglutinin stem as a broadly protective immunogen. *Science* 349: 1301–1306.
15. DiLillo, D. J., P. Palese, P. C. Wilson, and J. V. Ravetch. 2016. Broadly neutralizing anti-influenza antibodies require Fc receptor engagement for in vivo protection. *J. Clin. Invest.* 126: 605–610.
16. Hobson, D., R. L. Curry, A. S. Beare, and A. Ward-Gardner. 1972. The role of serum haemagglutination-inhibiting antibody in protection against challenge infection with influenza A2 and B viruses. *J. Hyg. (Lond.)* 70: 767–777.
17. Huber, V. C., J. M. Lynch, D. J. Bucher, J. Le, and D. W. Metzger. 2001. Fc receptor-mediated phagocytosis makes a significant contribution to clearance of influenza virus infections. *J. Immunol.* 166: 7381–7388.
18. Jegaskanda, S., E. R. Job, M. Kramski, K. Laurie, G. Isitman, R. de Rose, W. R. Winnall, I. Stratov, A. G. Brooks, P. C. Reading, and S. J. Kent. 2013. Cross-reactive influenza-specific antibody-dependent cellular cytotoxicity antibodies in the absence of neutralizing antibodies. *J. Immunol.* 190: 1837–1848.
19. Hung, I. F., K. K. To, C. K. Lee, K. L. Lee, W. W. Yan, K. Chan, W. M. Chan, C. W. Ngai, K. I. Law, F. L. Chow, et al. 2013. Hyperimmune IV immunoglobulin treatment: a multicenter double-blind randomized controlled trial for patients with severe 2009 influenza A(H1N1) infection. *Chest* 144: 464–473.
20. Chung, A. W., M. P. Kumar, K. B. Arnold, W. H. Yu, M. K. Schoen, L. J. Dunphy, T. J. Suscovich, N. Frahm, C. Linde, A. E. Mahan, et al. 2015. Dissecting polyclonal vaccine-induced humoral immunity against HIV using systems serology. *Cell* 163: 988–998.
21. Amigorena, S., D. Lankar, V. Briken, L. Gapin, M. Viguier, and C. Bonnerot. 1998. Type II and III receptors for immunoglobulin G (IgG) control the presentation of different T cell epitopes from single IgG-complexed antigens. *J. Exp. Med.* 187: 505–515.
22. Dhodapkar, K. M., J. L. Kaufman, M. Ehlers, D. K. Banerjee, E. Bonvini, S. Koenig, R. M. Steinman, J. V. Ravetch, and M. V. Dhodapkar. 2005. Selective blockade of inhibitory Fcgamma receptor enables human dendritic cell maturation with IL-12p70 production and immunity to antibody-coated tumor cells. *Proc. Natl. Acad. Sci. USA* 102: 2910–2915.
23. Maglione, P. J., J. Xu, A. Casadevall, and J. Chan. 2008. Fc gamma receptors regulate immune activation and susceptibility during *Mycobacterium tuberculosis* infection. *J. Immunol.* 180: 3329–3338.
24. DiLillo, D. J., and J. V. Ravetch. 2015. Differential Fc-receptor engagement drives an anti-tumor vaccinal effect. *Cell* 161: 1035–1045.
25. Oppenheim, D. E., R. Spreafico, A. Etuk, D. Malone, E. Amofah, C. Peña-Murillo, T. Murray, L. McLaughlin, B. S. Choi, S. Allan, et al. 2014. Glycoengineered anti-EGFR mAb elicits ADCC by NK cells from colorectal cancer patients irrespective of chemotherapy. *Br. J. Cancer* 110: 1221–1227.
26. Sliwkowski, M. X., and I. Mellman. 2013. Antibody therapeutics in cancer. *Science* 341: 1192–1198.
27. Lu, J., J. Chu, Z. Zou, N. B. Hamacher, M. W. Rixon, and P. D. Sun. 2015. Structure of FcγRI in complex with Fc reveals the importance of glycan recognition for high-affinity IgG binding. *Proc. Natl. Acad. Sci. USA* 112: 833–838.
28. Lu, J., J. L. Ellsworth, N. Hamacher, S. W. Oak, and P. D. Sun. 2011. Crystal structure of Fcγ receptor I and its implication in high affinity γ-immunoglobulin binding. *J. Biol. Chem.* 286: 40608–40613.
29. Maxwell, K. F., M. S. Powell, M. D. Hulett, P. A. Barton, I. F. McKenzie, T. P. Garrett, and P. M. Hogarth. 1999. Crystal structure of the human leukocyte Fc receptor, Fc gammaRIIa. *Nat. Struct. Biol.* 6: 437–442.
30. Ramsland, P. A., W. Farrugia, T. M. Bradford, C. T. Sardjono, S. Esparon, H. M. Trist, M. S. Powell, P. S. Tan, A. C. Cendron, B. D. Wines, et al. 2011. Structural basis for Fc gammaRIIa recognition of human IgG and formation of inflammatory signaling complexes. *J. Immunol.* 187: 3208–3217.
31. Sondermann, P., R. Huber, and U. Jacob. 1999. Crystal structure of the soluble form of the human fcgamma-receptor IIb: a new member of the immunoglobulin superfamily at 1.7 A resolution. *EMBO J.* 18: 1095–1103.
32. Radaev, S., S. Motyka, W. H. Fridman, C. Sautes-Fridman, and P. D. Sun. 2001. The structure of a human type III Fcgamma receptor in complex with Fc. *J. Biol. Chem.* 276: 16469–16477.
33. Sondermann, P., R. Huber, V. Oosthuizen, and U. Jacob. 2000. The 3.2-A crystal structure of the human IgG1 Fc fragment-Fc gammaRIII complex. *Nature* 406: 267–273.
34. Hogarth, P. M., and G. A. Pietersz. 2012. Fc receptor-targeted therapies for the treatment of inflammation, cancer and beyond. *Nat. Rev. Drug Discov.* 11: 311–331.
35. Albanesi, M., and M. Daëron. 2012. The interactions of therapeutic antibodies with Fc receptors. *Immunol. Lett.* 143: 20–27.
36. Nesspor, T. C., T. S. Raju, C. N. Chin, O. Vafa, and R. J. Brezski. 2012. Avidity confers FcγR binding and immune effector function to aglycosylated immunoglobulin G1. *J. Mol. Recognit.* 25: 147–154.
37. Bruhns, P., B. Iannascoli, P. England, D. A. Mancardi, N. Fernandez, S. Jorieux, and M. Daëron. 2009. Specificity and affinity of human Fcgamma receptors and their polymorphic variants for human IgG subclasses. *Blood* 113: 3716–3725.
38. Lux, A., X. Yu, C. N. Scanlan, and F. Nimmerjahn. 2013. Impact of immune complex size and glycosylation on IgG binding to human FcγRs. *J. Immunol.* 190: 4315–4323.
39. Acharya, P., W. D. Tolbert, N. Gohain, X. Wu, L. Yu, T. Liu, W. Huang, C. C. Huang, Y. D. Kwon, R. K. Louder, et al. 2014. Structural definition of an antibody-dependent cellular cytotoxicity response implicated in reduced risk for HIV-1 infection. *J. Virol.* 88: 12895–12906.
40. Cheng, Z. J., D. Garvin, A. Paguio, R. Moravec, L. Engel, F. Fan, and T. Surowy. 2014. Development of a robust reporter-based ADCC assay with frozen, thaw-and-use cells to measure Fc effector function of therapeutic antibodies. *J. Immunol. Methods* 414: 69–81.
41. Chung, S., Y. L. Lin, C. Reed, C. Ng, Z. J. Cheng, F. Malavasi, J. Yang, V. Quarmby, and A. Song. 2014. Characterization of in vitro antibody-dependent cell-mediated cytotoxicity activity of therapeutic antibodies - impact of effector cells. *J. Immunol. Methods* 407: 63–75.
42. Iida, S., R. Kuni-Kamochi, K. Mori, H. Misaka, M. Inoue, A. Okazaki, K. Shitara, and M. Satoh. 2009. Two mechanisms of the enhanced antibody-dependent cellular cytotoxicity (ADCC) efficacy of non-fucosylated therapeutic antibodies in human blood. *BMC Cancer* 9: 58.
43. Mata, M. M., F. Mahmood, R. T. Sowell, and L. L. Baum. 2014. Effects of cryopreservation on effector cells for antibody dependent cell-mediated cytotoxicity

(ADCC) and natural killer (NK) cell activity in (51)Cr-release and CD107a assays. *J. Immunol. Methods* 406: 1–9.
44. Mishima, Y., Y. Terui, Y. Mishima, R. Kuniyoshi, S. Matsusaka, M. Mikuniya, K. Kojima, and K. Hatake. 2012. High reproducible ADCC analysis revealed a competitive relation between ADCC and CDC and differences between FcγRIIIa polymorphism. *Int. Immunol.* 24: 477–483.
45. Tada, M., A. Ishii-Watabe, T. Suzuki, and N. Kawasaki. 2014. Development of a cell-based assay measuring the activation of FcγRIIa for the characterization of therapeutic monoclonal antibodies. *PLoS One* 9: e95787.
46. Howarth, M., K. Takao, Y. Hayashi, and A. Y. Ting. 2005. Targeting quantum dots to surface proteins in living cells with biotin ligase. *Proc. Natl. Acad. Sci. USA* 102: 7583–7588.
47. Ramsland, P. A., N. Willoughby, H. M. Trist, W. Farrugia, P. M. Hogarth, J. D. Fraser, and B. D. Wines. 2007. Structural basis for evasion of IgA immunity by *Staphylococcus aureus* revealed in the complex of SSL7 with Fc of human IgA1. *Proc. Natl. Acad. Sci. USA* 104: 15051–15056.
48. Hibbs, M. L., L. Bonadonna, B. M. Scott, I. F. C. McKenzie, and P. M. Hogarth. 1988. Molecular cloning of a human immunoglobulin G Fc receptor. *Proc. Natl. Acad. Sci. USA* 85: 2240–2244.
49. Patel, D., B. D. Wines, R. J. Langley, and J. D. Fraser. 2010. Specificity of staphylococcal superantigen-like protein 10 toward the human IgG1 Fc domain. *J. Immunol.* 184: 6283–6292.
50. Evans, M. J., S. L. Hartman, D. W. Wolff, S. A. Rollins, and S. P. Squinto. 1995. Rapid expression of an anti-human C5 chimeric Fab utilizing a vector that replicates in COS and 293 cells. *J. Immunol. Methods* 184: 123–138.
51. Petersen, T. N., S. Brunak, G. von Heijne, and H. Nielsen. 2011. SignalP 4.0: discriminating signal peptides from transmembrane regions. *Nat. Methods* 8: 785–786.
52. Jegaskanda, S., T. H. Amarasena, K. L. Laurie, H. X. Tan, J. Butler, M. S. Parsons, S. Alcantara, J. Petravic, M. P. Davenport, A. C. Hurt, et al. 2013. Standard trivalent influenza virus protein vaccination does not prime antibody-dependent cellular cytotoxicity in macaques. *J. Virol.* 87: 13706–13718.
53. Jegaskanda, S., K. L. Laurie, T. H. Amarasena, W. R. Winnall, M. Kramski, R. De Rose, I. G. Barr, A. G. Brooks, P. C. Reading, and S. J. Kent. 2013. Age-associated cross-reactive antibody-dependent cellular cytotoxicity toward 2009 pandemic influenza A virus subtype H1N1. *J. Infect. Dis.* 208: 1051–1061.
54. Jegaskanda, S., K. Vandenberg, K. L. Laurie, L. Loh, M. Kramski, W. R. Winnall, K. Kedzierska, S. Rockman, and S. J. Kent. 2014. Cross-reactive influenza-specific antibody-dependent cellular cytotoxicity in intravenous immunoglobulin as a potential therapeutic against emerging influenza viruses. *J. Infect. Dis.* 210: 1811–1822.
55. Gong, J. H., G. Maki, and H. G. Klingemann. 1994. Characterization of a human cell line (NK-92) with phenotypical and functional characteristics of activated natural killer cells. *Leukemia* 8: 652–658.
56. Lund, J., G. Winter, P. T. Jones, J. D. Pound, T. Tanaka, M. R. Walker, P. J. Artymiuk, Y. Arata, D. R. Burton, R. Jefferis, et al. 1991. Human Fc gamma RI and Fc gamma RII interact with distinct but overlapping sites on human IgG. *J. Immunol.* 147: 2657–2662.
57. Wines, B. D., M. S. Powell, P. W. Parren, N. Barnes, and P. M. Hogarth. 2000. The IgG Fc contains distinct Fc receptor (FcR) binding sites: the leukocyte receptors Fc gamma RI and Fc gamma RIIa bind to a region in the Fc distinct from that recognized by neonatal FcR and protein A. *J. Immunol.* 164: 5313–5318.
58. Golay, J., F. Da Roit, L. Bologna, C. Ferrara, J. H. Leusen, A. Rambaldi, C. Klein, and M. Introna. 2013. Glycoengineered CD20 antibody obinutuzumab activates neutrophils and mediates phagocytosis through CD16B more efficiently than rituximab. *Blood* 122: 3482–3491.
59. Metzger, H. 1992. Transmembrane signaling: the joy of aggregation. *J. Immunol.* 149: 1477–1487.
60. Greenberg, S., P. Chang, and S. C. Silverstein. 1994. Tyrosine phosphorylation of the γ subunit of Fcγ receptors, $p72^{syk}$, and paxillin during Fc receptor-mediated phagocytosis in macrophages. *J. Biol. Chem.* 269: 3897–3902.
61. Nimmerjahn, F., S. Gordan, and A. Lux. 2015. FcγR dependent mechanisms of cytotoxic, agonistic, and neutralizing antibody activities. *Trends Immunol.* 36: 325–336.
62. Glanville, J., W. Zhai, J. Berka, D. Telman, G. Huerta, G. R. Mehta, I. Ni, L. Mei, P. D. Sundar, G. M. Day, et al. 2009. Precise determination of the diversity of a combinatorial antibody library gives insight into the human immunoglobulin repertoire. *Proc. Natl. Acad. Sci. USA* 106: 20216–20221.
63. Boesch, A. W., E. P. Brown, H. D. Cheng, M. O. Ofori, E. Normandin, P. A. Nigrovic, G. Alter, and M. E. Ackerman. 2014. Highly parallel characterization of IgG Fc binding interactions. *MAbs* 6: 915–927.
64. Ackerman, M. E., M. Crispin, X. Yu, K. Baruah, A. W. Boesch, D. J. Harvey, A. S. Dugast, E. L. Heizen, A. Ercan, I. Choi, et al. 2013. Natural variation in Fc glycosylation of HIV-specific antibodies impacts antiviral activity. *J. Clin. Invest.* 123: 2183–2192.
65. Ackerman, M. E., A. S. Dugast, E. G. McAndrew, S. Tsoukas, A. F. Licht, D. J. Irvine, and G. Alter. 2013. Enhanced phagocytic activity of HIV-specific antibodies correlates with natural production of immunoglobulins with skewed affinity for FcγR2a and FcγR2b. *J. Virol.* 87: 5468–5476.
66. Barouch, D. H., G. Alter, T. Broge, C. Linde, M. E. Ackerman, E. P. Brown, E. N. Borducchi, K. M. Smith, J. P. Nkolola, J. Liu, et al. 2015. Protective efficacy of adenovirus/protein vaccines against SIV challenges in rhesus monkeys. *Science* 349: 320–324.
67. Ackerman, M. E., A. Mikhailova, E. P. Brown, K. G. Dowell, B. D. Walker, C. Bailey-Kellogg, T. J. Suscovich, and G. Alter. 2016. Polyfunctional HIV-specific antibody responses are associated with spontaneous HIV control. *PLoS Pathog.* 12: e1005315.
68. Brown, E. P., A. F. Licht, A. S. Dugast, I. Choi, C. Bailey-Kellogg, G. Alter, and M. E. Ackerman. 2012. High-throughput, multiplexed IgG subclassing of antigen-specific antibodies from clinical samples. *J. Immunol. Methods* 386: 117–123.
69. Chung, S., V. Quarmby, X. Gao, Y. Ying, L. Lin, C. Reed, C. Fong, W. Lau, Z. J. Qiu, A. Shen, et al. 2012. Quantitative evaluation of fucose reducing effects in a humanized antibody on Fcγ receptor binding and antibody-dependent cell-mediated cytotoxicity activities. *MAbs* 4: 326–340.
70. Chung, A. W., M. Ghebremichael, H. Robinson, E. Brown, I. Choi, S. Lane, A. S. Dugast, M. K. Schoen, M. Rolland, T. J. Suscovich, et al. 2014. Polyfunctional Fc-effector profiles mediated by IgG subclass selection distinguish RV144 and VAX003 vaccines. *Sci. Transl. Med.* 6: 228ra38.
71. Dutta, K., A. K. Varshney, M. C. Franklin, M. Goger, X. Wang, and B. C. Fries. 2015. Mechanisms mediating enhanced neutralization efficacy of staphylococcal enterotoxin B by combinations of monoclonal antibodies. *J. Biol. Chem.* 290: 6715–6730.
72. Bakker, A. B., C. Python, C. J. Kissling, P. Pandya, W. E. Marissen, M. F. Brink, F. Lagerwerf, S. Worst, E. van Corven, S. Kostense, et al. 2008. First administration to humans of a monoclonal antibody cocktail against rabies virus: safety, tolerability, and neutralizing activity. *Vaccine* 26: 5922–5927.
73. Lowy, I., D. C. Molrine, B. A. Leav, B. M. Blair, R. Baxter, D. N. Gerding, G. Nichol, W. D. Thomas, Jr., M. Leney, S. Sloan, et al. 2010. Treatment with monoclonal antibodies against *Clostridium difficile* toxins. *N. Engl. J. Med.* 362: 197–205.
74. Qiu, X., G. Wong, J. Audet, A. Bello, L. Fernando, J. B. Alimonti, H. Fausther-Bovendo, H. Wei, J. Aviles, E. Hiatt, et al. 2014. Reversion of advanced Ebola virus disease in nonhuman primates with ZMapp. *Nature* 514: 47–53.